

Studies on the Distribution of Calretinin in the Rabbit Midcingulate Cortex

(ウサギ中部帯状皮質におけるカルレチニンの分布に関する研究)

2018

The United Graduate School of Veterinary Sciences, Gifu University
(Tokyo University of Agriculture and Technology)

Mohi Uddin

Studies on the Distribution of Calretinin in the Rabbit Midcingulate Cortex

(ウサギ中部帯状皮質におけるカルレチニンの分布に関する研究)

Mohi Uddin

CONTENTS

Introduction	1
Materials and Methods.....	3
Results	6
Discussion	9
Conclusions	13
Summary	14
Acknowledgments.....	15
References	16
Figures	25
Tables	35

Abbreviations

aMCC	anterior midcingulate cortex
ACC	anterior cingulate cortex
CR	calretinin
DAB	3,3'-diaminobenzidine tetrahydrochloride
GABA	gamma aminobutyric acid
L	layer
MCC	midcingulate cortex
NeuN	neuronal nuclear protein
pMCC	posterior midcingulate cortex
TBS	Tris-HCl-buffered saline
U.S.A.	United States of America
+	immunopositive

INTRODUCTION

The mammalian neocortex encompasses neurons that are intricately organized in laminar and columnar fashions (31, 42, 54). Neocortical neuronal populations are categorized into two distinct groups. The first group includes excitatory neurons that represent nearly 80% of the total cortical neuronal populations (54) and usually use glutamate as a neurotransmitter (31, 42). The other group encloses inhibitory neurons that represent around 20% of the total cortical neurons (54) and commonly use gamma aminobutyric acid (GABA) as a neurotransmitter (22, 33, 57). Cortical neuronal circuits are formed by excitatory glutamatergic neurons or principal neurons that provide axons to particular cortical and subcortical areas in the central nervous system (31, 42), and inhibitory GABAergic neurons that provide their processes usually within the cortical area including the somata of these neurons (31, 51).

Inhibitory GABAergic neurons play essential roles in normal functioning of the central nervous system (37). They regulate information flow in the cortex by influencing the excitatory activity of principal neurons and thereby regulating the timing of their firing to adjust the excitatory and inhibitory balance that is essential for the neuronal information processing (25, 37, 38, 48, 70). Dysfunction of these inhibitory neurons may lead various neurological diseases such as epilepsy, schizophrenia, and autism (9, 10, 24, 35). Therefore, the knowledge of the organization of inhibitory GABAergic neurons is crucial to understand neuronal information processing within the neocortex (40, 49).

Inhibitory GABAergic neurons can be demarcated by their morphology, physiology, and neurochemical substances that they express (2, 12, 22, 37). Calcium binding proteins are considered to be excellent neurochemical markers to characterize the organization of inhibitory GABAergic neurons in neocortical areas (3, 28, 43). Among many calcium binding proteins, calretinin (CR), which is a member of EF hand family (20, 36,

53), is expressed in a morphologically distinct subpopulation of inhibitory GABAergic neurons that are intimately linked to cortical functions (22, 30, 33, 72). The distribution of CR immunopositive (+) neurons differs among different neocortical areas (28, 29, 45). Hence, CR is considered to be an excellent neurochemical marker to characterize neocortical areas (3, 28, 43).

The midcingulate cortex (MCC) in the rabbit is designated as area 24' which resides in the mid-rostrocaudal part of the cingulate gyrus (62). In the rabbit, the MCC is well developed and highly differentiated (62, 63), and plays essential roles in various cognitive functions such as response selection, error detection, and discriminative avoidance behavior (19, 55). A previous cytoarchitectural study with Nissl staining demonstrated that the rabbit MCC consists of two areas: area 24a' ventrally and area 24b' dorsally (62). A later study based on the distribution of several neurochemical markers including calcium-binding protein parvalbumin suggested that area 24a' is subdivided into anterior area a24a' and posterior area p24a', and area 24b' is subdivided into anterior area a24b' and posterior area p24b' (63). This parcellation pattern in the rabbit is more similar to that found in humans compared to the rodent parcellation (60, 66, 73).

The MCC is of great importance in human nociceptive, cognitive, and skeletomotor functions (64). Several studies in humans have shown that the anterior MCC (aMCC) is critically involved in avoidance behaviors (67), emotions such as anger and hostility (14, 41), and cognitive performance tasks such as response selection and error detection (4, 5, 47). In contrast, the posterior MCC (pMCC) is involved in guiding body orientation and reflexive movements (67), and pain processing (32). In altered conditions, aMCC is intimately linked to several diseases such as frontotemporal dementia (8) and obsessive-compulsive disorder (52), whereas pMCC is involved in progressive supranuclear palsy (8). The differences between the aMCC and pMCC in functional

involvement and susceptibility in human disorders heighten the need to develop experimental animal models for studies of physiology and disorder mechanisms linked to the human MCC.

The rabbit may be used as an experimental model for pathophysiological studies related to the human MCC, since its MCC parcellation pattern is more similar to that of humans than that of rodents as mentioned above. Although the structural organization has been studied with several neurochemical markers in the rabbit (63), more detailed studies are needed to characterize the similarities and differences in the distribution of other neuronal substances between each area of the MCC.

To better understand the neuronal organization of the MCC areas, I immunohistochemically observed CR⁺ structures, which has hitherto not yet been explored in the MCC of the rabbit. Moreover, the distribution and morphology of CR⁺ neurons differ from PV⁺ neurons in the neocortex (11, 28, 29, 45). Therefore, I assumed that the comprehensive neuromorphological and neurochemical characterization of the MCC areas is crucial and useful for future morphological and functional studies to further understanding of areal contributions to the different aspect of MCC functions.

MATERIALS AND METHODS

All animal handling and experimental protocols were approved by the Ethics Committee of Animal Experimentation of Tokyo University of Agriculture and Technology and complied with the guideline for the care and use of laboratory animals at Tokyo University of Agriculture and Technology and National Institutes of Health.

Collection and fixation of brains

Five adult male New Zealand White rabbits (2.35-2.70 kg) were used in this study. All the experimental animals were healthy on physical examinations. These animals were anaesthetized with intramuscular injection of xylazine (10 mg/kg body weight) and intraperitoneal injection of pentobarbital sodium (60 mg/kg body weight), and initially perfused through the ascending aorta with 1 l of 0.9% NaCl, followed by 1.5-2.0 l of 4% paraformaldehyde in 0.1 M phosphate buffer (pH 7.4). After perfusion, connective tissue, muscles, and bones around the cranial cavity were removed to extract the brains from the cranium. After obtained the brains from the cranial cavity, they were placed in the same fixative for post-fixation at 4°C for 2-5 h.

Tissue processing

For cryoprotection, brains were shifted into vials containing 30% sucrose in 0.1 M phosphate buffer and kept them in the refrigerator at 4°C with mild shaking for 48 h until the brains sank to the bottom of the vials. Afterward, the brains were sectioned on a freezing microtome at 50 μ m thickness in the coronal plane and divided into five series. Two of these series were used for the present study, while the remaining series were used for other studies. After sectioning, the sections were preserved in Tris-HCl-buffered saline (TBS) (pH 7.6) containing 0.01% sodium azide before immunohistochemical treatment.

Immunohistochemistry of calretinin

One series of sections were chosen for CR immunohistochemistry. Initially, free-floating sections were dealt with a solution containing 0.3 % H₂O₂ in ethanol-TBS (1:1) to eliminate endogenous peroxidase activity and then washed three times with TBS (5 min each). After that, the sections were transferred to TBS containing 1% normal horse

serum and 0.5% Triton-X-100 and incubated overnight at 4°C to block nonspecific antibody binding to the tissue. Next, the primary antibody incubation was performed at 4°C for 48 h in TBS containing 0.5% Triton-X-100, 1% normal horse serum, and mouse monoclonal primary antibody raised against CR (1:2,000 or 8,000; clone 6B8.2 Cat.# MAB 1568, Merck Millipore, Darmstadt, Germany). After incubation, the sections were rinsed three times with TBS (5 min each), followed by incubation in TBS containing 0.5% Triton-X-100, 1% normal horse serum, and biotinylated horse anti-mouse IgG (1:600; Vector Laboratories, Burlingame, California, U.S.A.) at room temperature for 1 h. Next, the sections were washed three times with TBS (5 min each) and incubated in avidin-biotinylated horseradish peroxidase (1:100; Vector Laboratories) in TBS at room temperature for 1 h. Afterward, the sections were rinsed three times with TBS (5 min each) and then treated with TBS containing 0.04% 3,3'-diaminobenzidine tetrahydrochloride (DAB) and 0.01% H₂O₂. After rinsing three times in TBS, the sections were mounted on gelatin-coated slides and dried overnight at room temperature. Thereafter, to remove lipids from the tissue, the sections were soaked in a mixture of 100% chloroform and 100% ethanol (1:1 ratio, two steps) for 30 min in each step at room temperature, and, next, dehydrated in ethanols (three steps in 100% ethanol; 5 min each step). Afterward, the sections were cleared with xylene (three steps; 5 min each step) and coverslipped with Permount (Fisher Scientific, Fair Lawn, New Jersey, U.S.A.).

Another series of sections were treated with 1:10,000 antibody against the neuronal nuclear protein (NeuN) (Chemicon International, Temecula, California, U.S.A.) in TBS for 48 h at 4°C with a similar procedure for the identification of boundaries of each area and the cortical layer of the MCC.

Counting of CR + somata and statistical analysis

Three cases were selected at random for semiquantitative analysis. Eight representative sections with 200 μm intervals were chosen from each case. Before counting, the boundaries of cortical layers in CR stained sections were drawn and layers were identified as layer (L) 1, L2/3, L5, and L6, with the aid of NeuN stained sections and according to the description of Vogt (63). The counting was systematically conducted with a 20-times objective lens using an Eclipse-Ni photomicroscope (Nikon Instruments, Tokyo, Japan) linked to NIS-Elements (ver. 4.2) image analysis software (Nikon Instruments). The data were collected, and the density was calculated with Microsoft Excel 2016 (Microsoft Corporation, Redmond, Washington, U.S.A.). The number and densities of positive somata in four areas were compared using analysis of variance, followed by Bonferroni's multiple comparisons. $P < 0.05$ was considered to be statistically significant.

Image acquisition and processing

Images of selected sections were captured with a DS-Ri1 digital sight camera (Nikon Instruments) controlled with NIS-Elements (ver. 4.2) image analysis software (Nikon Instruments). The images were adjusted to attain optimal resolution, brightness, contrast, and sharpness, and trimmed with Adobe Photoshop CC (Adobe Systems, San Jose, California, U.S.A.). Afterwards, the adjusted images were assembled into Figures with Adobe Illustrator CC (Adobe Systems).

RESULTS

In the MCC, CR⁺ somata consisted of many multipolar and some bipolar types, and CR⁺ fibers were composed of dendrites, axons, and terminals. Throughout the MCC areas, CR⁺ somata were mostly distributed in L2/3 and L6, whereas CR⁺ fibers in L1,

L2/3, and L6. However, the CR⁺ somata and fibers showed areal as well as laminar preferential distributions in each area of the MCC.

CR immunoreactivity in area a24a'

Area a24a' (Figs. 1a, 1a', and 2a) contained the greatest number of CR⁺ somata among all areas of the MCC (Fig. 3 and Table 1). Within this area, approximately 57% of the entire CR⁺ somata occurred in L2/3 and 29% in L6, whereas fewer CR⁺ somata were observed in L5 (12%) and L1 (3%) (Table 1). The number of CR⁺ somata in area a24a' was significantly higher than the other areas of the MCC (Fig. 3). The density of CR⁺ somata in this area tended to be higher than that in area p24a' and was significantly higher than those in area a24b' and area p24b' (Fig. 4 and Table 2). The difference in number was attributable mainly to that in the total number of multipolar somata and of somata of each layer (Fig. 3), whereas the difference in density was attributable mainly to that in the total number of multipolar and L2/3 somata (Fig. 4). In area a24a', the number and density were high in L2/3 and L6, but low in L1 and L5 (Tables 1 and 2). In CR⁺ somata, non-pyramidal multipolar neurons were predominant across all layers of the MCC (Figs. 2a, 5a, and 5b, and Tables 1 and 2).

In L1 of area a24a', only a few CR⁺ multipolar neurons were observed (Figs. 2a, 5a, and 5b, and Tables 1 and 2). In L2/3, CR⁺ multipolar and bipolar neurons were mostly distributed in the superficial part, while in deep L2/3, fewer CR⁺ somata were scattered (Fig. 2a). The multipolar neurons had oval, round, or triangular somata with multiple dendrites directing various directions depending on each cell (Fig. 5a and 5b). The bipolar neurons had oval or fusiform somata and two vertically oriented dendritic arbors arising from the superficial and deep somatic poles (Fig. 5a). L5 and L6 contained mostly CR⁺ multipolar and a few bipolar somata (Fig. 2a, and Tables 1 and 2).

The distribution of these types of neurons had laminar preference, but no areal preference across all areas of the MCC.

In area a24a', CR+ fibers were most abundant in L1 (Figs. 2a and 5c), followed by L6, L5, and L2/3 in decreasing order. CR+ fibers running almost rostrocaudally were also present in the cingulum, deep to L6 (Fig. 2a). In L1 of area a24a', most CR+ fibers coursed almost parallel to the pial surface in the superficial part to provide terminals to that part (Figs. 2a and 5c). CR+ dendritic processes also ran almost vertically in L1. In some cases, these processes were able to be traced to the multipolar and bipolar somata that were located mostly in L2/3. In L2/3, the majority of CR+ dendritic processes coursed vertically, and some showed a beaded appearance (Fig. 5b). In rare cases, the beaded processes were found to be issued from the multipolar or bipolar somata located mainly in L2/3 (Fig. 5b). In L5 and L6, CR+ fibers were directed randomly. In each of L2/3, L5, and L6, the distribution of CR+ fibers was relatively uniform across the laminar thickness.

CR+ immunoreactivity in area p24a'

In area p24a', the pattern of distribution of CR+ somata was similar to that in area a24a', but the number of CR+ somata in the total layers and each layer of area p24a' was significantly lower than that of area a24a' (Fig. 3 and Table 1). The density of CR+ somata in area p24a' tended to be lower than that in area a24a' and was significantly higher than that in areas a24b' and p24b' (Fig. 4 and Table 2). In L2/3 of area p24a', CR+ multipolar and bipolar somata were distributed throughout the thickness of L2/3 (Fig. 2b), unlike that of area a24a'.

Area p24a' enclosed more abundant CR+ dendrites, axons and terminals than area a24a' in all cortical layers (Figs. 2b and 5d), with a similar distribution pattern to area

a24a'. Moreover, the deep part of L2/3 in area p24a' enclosed patchy CR+ fibers (arrows in Figs. 2b and 5e) that ran mostly parallel to the pial surface and provided axon terminals (Fig. 5f), while this feature was lacking in area a24a' (Fig. 2a).

CR+ immunoreactivity in area a24b'

In area a24b', the laminar distribution pattern of CR+ somata and fibers was again similar to those in area a24a' (Fig. 2a and 2c). The total number and density of CR+ somata tended to be larger than those of area p24b' (Figs. 3 and 4, and Tables 1 and 2). Among the MCC areas, area a24b' generally contained the fewest CR+ fibers in all cortical layers (Fig. 2c).

CR+ immunoreactivity in area p24b'

In area p24b', the laminar distribution pattern of CR+ somata was similar to that in area p24a' (Fig. 2b and 2d). Across all layers, the CR+ somal number and density tended to be smallest in area p24b' compared to other areas of the MCC (Figs. 3 and 4, and Tables 1 and 2). Like area p24a', patchy CR+ fibers with axon terminals occurred in deep L2/3, but this feature was less prominent than that of area p24a' (Fig. 2b and 2d).

DISCUSSION

The present study demonstrated that the distribution of CR+ somata and fibers in each area of the rabbit MCC differed from each other. The present findings greatly characterize each area of the MCC more than a previous study using another calcium-binding protein PV by Vogt (63), who showed only a tendency that area a24a' had fewer PV+ neurons than area p24a'.

Distributions of CR+ somata

Most CR+ somata in the MCC are located in L2/3 and L6, while there are fewer in L5 and fewest in L1. This distribution pattern has not previously been reported in any cortical area of any other species. In the anterior cingulate cortex (ACC) of the cingulate gyrus, previous immunohistochemical studies have shown that CR+ somata were observed mainly in L2/3 in the rat (17), cynomolgus monkey (15, 16), and humans (18). In the visual cortex, CR+ somata are also present mainly in L2/3 in the rabbit (55), mouse (44), hamster (34), dog (27), and cynomolgus monkey (39), whereas they are located in L1 and L2 in the bottlenose dolphin, L2/3 and L4a-c in humans (21), and L2/3, followed by L5, L6, L4, and L1 in decreasing order in the rat (22). Although these studies show that neocortical areas tend to have numerous CR+ somata in L2/3 in many mammalian species, the rabbit MCC is characterized by the finding that L6 also has many CR+ somata.

Morphology of CR+ somata

In the rabbit MCC, CR is expressed in non-pyramidal multipolar and bipolar neurons and the non-pyramidal multipolar neurons are predominant in any layer of any area. Although there have not been any similar previous studies in the MCC of other species, the present findings are in contrast to previous findings in the ACC of the cingulate gyrus, where bipolar and bitufted somata are predominant over multipolar somata in the rat (17), monkey (15), and humans (18). In the visual cortex, it is also reported that bipolar somata are predominant over multipolar somata in the rabbit (45), mouse (44), and hamsters (34), whereas the two types are even in the rat (22). Therefore, although in the neocortical areas in most mammalian species studied, CR+ neurons are mainly of bipolar and bitufted neurons, the rabbit MCC is peculiar in that CR+ neurons consist predominantly of the multipolar type.

Distribution of CR+ fibers

There is a tendency that CR+ neuropil staining is more abundant posteriorly than anteriorly in the MCC. CR+ fibers were most abundant in L1, especially its superficial part, followed by L6, L5, and L2/3 in decreasing order. Deep L2/3 of areas p24a' and p24b' also contains patchy CR+ fibers, which are absent in areas a24a' and a24b'. These patterns of the distribution of CR+ fibers have been demonstrated for the first time in the MCC, and differ from the pattern in other regions of the cingulate gyrus in other mammalian species, where CR+ fibers are distributed homogeneously. For example, in the ACC of the rat, L1 was stained darker than the other layers, but no sublaminal preference of CR+ fibers was described within L1 (29). In the ACC of monkeys and humans, the distribution of CR+ fibers was stained homogeneously across layers, except that deep L1 stained intensely in humans, but not so in monkeys (29).

Although there is no direct evidence for the existence of cells of origin of CR+ fibers observed in the MCC of the rabbit, previous hodological and immunohistochemical studies in this and other species may provide some clues to know the CR+ fiber architecture. As most CR+ neurons are a subpopulation of GABAergic neurons (23, 33), it is considered that most, if not all, CR+ fibers in the MCC may be of intrinsic origins (6, 11). Furthermore, given the existence of long-range GABAergic projections between cortical areas (26, 56, 58), part of the CR+ fibers and terminals in L1 and L5 may correspond to those of the projections originating from retrosplenial area 30 to the MCC (61). Other CR+ fibers and terminals that occur in patches in L2/3 of areas p24a' and p24b' may also originate from within or outside of the MCC, but no previous studies have addressed this issue so far.

Some CR+ fibers may have subcortical origins; CR+ fibers in L1 may originate from the thalamus, since many somata that were positive for CR immunoreactivity and CR mRNA were observed in the rat in the midline thalamus including nucleus reuniens and rhomboideus (1, 50, 71). It is also reported that nucleus reuniens give rich terminals to L1 and nucleus rhomboideus to all layers of the MCC in the rat (59). Therefore, it is assumed that in the rabbit MCC, CR+ fibers of L1 and some other layers may contain CR+ thalamocortical fibers originating from CR+ somata in nucleus reuniens and rhomboideus.

Characterization of the rabbit MCC

There are some differences in the CR+ somata/fibers distribution in each area; CR+ somata occur in superficial L2/3 of areas a24a' and a24b', while they were distributed in entire L2/3 of areas p24a' and p24b'. There was a general tendency that CR+ somal density was highest in area a24a', followed by area p24a', area a24b' and area p24b' in decreasing order. CR+ fibers were most abundant in area p24a', followed by area p24b', area a24a' and area a24b' in decreasing order. These differences in the distribution of CR+ somata and fibers suggest that each area may be anatomically distinct. Moreover, the present findings support the anteroposterior and ventrodorsal parcellation of the rabbit MCC (63), which is similar to that of humans (60, 65, 73) and monkeys (65, 68). In rodents, the ventrodorsal parcellation of the MCC is noted (46, 64, 66, 69), whereas the anteroposterior parcellation is lacking (64, 66). Hence, the present study supports the notion that the MCC of humans is more similar to the MCC of rabbits than that of rodents. Although the distribution of CR+ structures in the MCC has not been studied in humans so far, the relative similarity of the MCC parcellation pattern between the rabbit and humans underpins the idea that the rabbit may serve as a more suitable experimental

model for pathophysiological studies of, at a minimum, parts of the human MCC than rodents.

Functional significance

CR+ neurons are a subpopulation of inhibitory GABAergic neurons in the neocortex of the rat and mouse (22, 33, 72). It is generally assumed that CR+ multipolar neurons may provide information in a transcolumnar fashion in the cortex (6), whereas CR+ bipolar neurons may integrate it within a columnar structure (6, 49). This may hold true for CR+ multipolar and bipolar neurons in the MCC of the rabbit. Since CR+ neurons occur not only in L2/3 as in other cingulate areas in rodents (17), but also in L6, and CR+ multipolar neurons are distributed more densely than bipolar neurons, CR+ neurons in the MCC may be involved in more complex information processing by integrating signals within a column as well as receiving/sending signals from/to nearby columns. CR+ fibers, some of which may be of extrinsic cortical and/or thalamic origins, may also modulate neuronal activity in the MCC. Therefore, in the rabbit MCC, CR+ neurons and CR+ fibers originating from inside and/or outside of the MCC may be involved in information processing more peculiar and complex way, in comparison with other cingulate cortical areas in rodents (17). There may be some possible differences in information processing in each area of the MCC. This issue should be addressed in future studies.

CONCLUSIONS

The present immunohistochemical study using CR as a marker demonstrates that each constituent area of the rabbit MCC (area a24a', area p24a', area a24b', and area p24b') is characterized by a unique set of the existence of CR+ somata and fibers, sug-

gesting that CR+ neurons may contribute to information processing for cognitive functions in somewhat different manners in each area of the rabbit MCC.

SUMMARY

The midcingulate cortex (MCC; area 24') resides in the mid-rostrocaudal part of the cingulate gyrus, and it plays important roles in nociceptive, cognitive, and skeletomotor functions. The MCC has recently been shown to consist of four cortical areas (areas a24a', a24b', p24a', and p24b') in the rabbit, based on immunohistochemistry. To further characterize the organization of these areas, the present study immunohistochemically identified structures immunopositive (+) for calretinin (CR) as a marker of a subpopulation of inhibitory neurons. CR⁺ somata were identified as multipolar and bipolar neurons. The multipolar neurons were predominant throughout the MCC. CR⁺ somata were present mainly in layer (L) 2/3 and L6, and CR⁺ fibers occurred mainly in L1, L2/3 and L6. However, there were differences in the distribution of CR⁺ structures in each area. CR⁺ somata tended to be most densely distributed in area a24a', followed by area p24a', area a24b' and area p24b'. CR⁺ fibers were most densely distributed in area p24a', followed by area p24b', area a24a' and area a24b'. In addition, only areas p24a' and p24b' enclosed patchy CR⁺ fibers and terminals in deep L2/3. These results show the distinct distribution of CR⁺ structures in each area of the MCC in the rabbit, suggesting that CR⁺ neurons may contribute to information processing for cognitive functions in somewhat different manners in each area of the MCC.

ACKNOWLEDGMENTS

First of all, I would like to pray and express my cordial gratefulness and acknowledgment to the Magnificent and the Almighty ALLAH who gave me the capability and the power to carried out this work.

I want to express my deepest gratitude, cordial and sincere thanks to my supervisor and mentor Professor Dr. Hideshi Shibata, Laboratory of Veterinary Anatomy, Department of Veterinary Medicine, Faculty of Agriculture, Tokyo University of Agriculture and Technology for admitting me to be a member of his lab to explore the neuroanatomy. I am very grateful for this learning opportunity and the skills which will be vital tools to build my future career. Besides, he has been a great supportive mentor who always helped me to achieve my goals and aspirations by offering consistent guidance and advice. Professor Shibata's philosophies and comments have been inspiring and motivating, and fundamental for the completion of this thesis.

I am also cordially gratefully to Professor Dr. Gen Watanabe at Tokyo University of Agriculture and Technology, Professor Dr. Yoshio Yamamoto at Iwate University, Professor Dr. Motoki Sasaki at Obihiro University of Agriculture and Veterinary Medicine and Associate Professor Dr. Shioichiro Saito at Gifu University for their supervisions and continuous encouragements throughout the course of this study.

I would like to thanks to all of my lab members specially Tetsuhito Kigata and Ahmed Faisal Amiry for their support during perfusion of animals and other laboratory procedures.

My family members, beloved spouse and son also deserve the deepest thanks for their support and inspirations in my life and during my study.

REFERENCES

- 1) Arai, R., Jacobowitz, D. M. and Deura, S. (1994). Distribution of calretinin, calbindin-D28k, and parvalbumin in the rat thalamus. *Brain Res. Bull.* 33, 595~614.
- 2) Ascoli, G. A., Alonso-Nanclares, L., Anderson, S. A., Barrionuevo, G., Benavides-Piccione, R., Burkhalter, A., Buzsáki, G., Cauli, B., Defelipe, J., Fairén, A., Feldmeyer, D., Fishell, G., Fregnac, Y., Freund, T. F., Gardner, D., Gardner, E. P., Goldberg, J. H., Helmstaedter, M., Hestrin, S., Karube, F., Kisvárdy, Z. F., Lambolez, B., Lewis, D. A., Marin, O., Markram, H., Muñoz, A., Packer, A., Petersen, C. C. H., Rockland, K. S., Rossier, J., Rudy, B., Somogyi, P., Staiger, J. F., Tamas, G., Thomson, A. M., Toledo-Rodriguez, M., Wang, Y., West, D. C. and Yuste, R. (2008). Petilla terminology: nomenclature of features of GABAergic interneurons of the cerebral cortex. *Nat. Rev. Neurosci.* 9, 557~568.
- 3) Barinka, F. and Druga, R. (2010). Calretinin expression in the mammalian neocortex: A review. *Physiol. Res.* 59, 665~677.
- 4) Bush, G., Vogt, B. A., Holmes, J., Dale, A. M., Greve, D., Jenike, M. A. and Rosen, B. R. (2002). Dorsal anterior cingulate cortex: a role in reward-based decision making. *Proc. Natl. Acad. Sci. U. S. A.* 99, 523~528.
- 5) Bush, G., Whalen, P. J., Rosen, B. R., Jenike, M. A., McInerney, S. C. and Rauch, S. L. (1998). The counting stroop: An interference task specialized for functional neuroimaging-validation study with functional MRI. *Hum. Brain Mapp.* 6, 270~282.
- 6) Cauli, B., Zhou, X., Tricoire, L., Toussay, X. and Staiger, J. F. (2014). Revisiting enigmatic cortical calretinin-expressing interneurons. *Front. Neuroanat.* 8, 1~18.
- 7) Cheron, G., Servais, L., Dan, B., Gall, D., Roussel, C. and Schiffmann, S. N. (2005). Fast oscillation in the cerebellar cortex of calcium binding protein-deficient mice: a new sensorimotor arrest rhythm. *Prog. Brain Res.* 148, 165~180.

- 8) Chiu, W. Z., Papma, J. M., de Koning, I., Donker Kaat, L., Seelaar, H., Reijls, A. E. M., Valkema, R., Hasan, D., Boon, A. J. W. and van Swieten, J. C. (2012). Midcingulate involvement in progressive supranuclear palsy and tau positive frontotemporal dementia. *J. Neurol. Neurosurg. Psychiatry.* 83, 910~915.
- 9) Cobos, I., Calcagnotto, M. E., Vilaythong, A. J., Thwin, M. T., Noebels, J. L., Baraban, S. C. and Rubenstein, J. L. R. (2005). Mice lacking *Dlx1* show subtype-specific loss of interneurons, reduced inhibition and epilepsy. *Nat. Neurosci.* 8, 1059~1068.
- 10) Cossart, R., Dinocourt, C., Hirsch, J. C., Merchan-Perez, A., De Felipe, J., Ben-Ari, Y., Esclapez, M. and Bernard, C. (2001). Dendritic but not somatic GABAergic inhibition is decreased in experimental epilepsy. *Nat. Neurosci.* 4, 52~62.
- 11) DeFelipe, J. (1997). Types of neurons, synaptic connections and chemical characteristics of cells immunoreactive for calbindin-D28K, parvalbumin and calretinin in the neocortex. *J. Chem. Neuroanat.* 14, 1~19.
- 12) DeFelipe, J., López-Cruz, P. L., Benavides-Piccione, R., Bielza, C., Larrañaga, P., Anderson, S., Burkhalter, A., Cauli, B., Fairén, A., Feldmeyer, D., Fishell, G., Fitzpatrick, D., Freund, T. F., González-Burgos, G., Hestrin, S., Hill, S., Hof, P. R., Huang, J., Jones, E. G., Kawaguchi, Y., Kisvárdy, Z., Kubota, Y., Lewis, D. A., Marín, O., Markram, H., McBain, C. J., Meyer, H. S., Monyer, H., Nelson, S. B., Rockland, K., Rossier, J., Rubenstein, J. L. R., Rudy, B., Scanziani, M., Shepherd, G. M., Sherwood, C. C., Staiger, J. F., Tamás, G., Thomson, A., Wang, Y., Yuste, R. and Ascoli, G. A. (2013). New insights into the classification and nomenclature of cortical GABAergic interneurons. *Nat. Rev. Neurosci.* 14, 202~216.
- 13) D'Orlando, C., Celio, M. and Schwaller, B. (2002). Calretinin and calbindin D-28k, but not parvalbumin protect against glutamate-induced delayed excitotoxicity in

- transfected N18-RE 105 neuroblastoma-retina hybrid cells. *Brain Res.* 945, 181~190.
- 14) Dougherty, D. D., Shin, L. M., Alpert, N. M., Pitman, R. K., Orr, S. P., Lasko, M., Macklin, M. L., Fischman, A. J. and Rauch, S. L. (1999). Anger in healthy men: a PET study using script-driven imagery. *Biol. Psychiatry.* 46, 466~472.
 - 15) Gabbott, P. L. A. and Bacon, S. J. (1996). Local circuit neurons in the medial prefrontal cortex (areas 24a,b,c, 25 and 32) in the monkey: I. Cell morphology and morphometrics. *J. Comp. Neurol.* 364, 567~608.
 - 16) Gabbott, P. L. A. and Bacon, S. J. (1996). Local circuit neurons in the medial prefrontal cortex (areas 24a,b,c, 25 and 32) in the monkey: II. Quantitative areal and laminar distributions. *J. Comp. Neurol.* 364, 609~636.
 - 17) Gabbott, P. L. A., Dickie, B. G. M., Vaid, R. R., Headlam, A. J. N. and Bacon, S. J. (1997). Local-circuit neurones in the medial prefrontal cortex (areas 25, 32 and 24b) in the rat: Morphology and quantitative distribution. *J. Comp. Neurol.* 377, 465~499.
 - 18) Gabbott, P. L. A., Jays, P. R. L. and Bacon, S. J. (1997). Calretinin neurons in human medial prefrontal cortex (areas 24a,b,c, 32', and 25). *J. Comp. Neurol.* 381, 389~410.
 - 19) Gabriel, M., Kubota, Y., Sparenborg, S., Straube, K. and Vogt, B. A. (1991). Effects of cingulate cortical lesions on avoidance learning and training-induced unit activity in rabbits. *Exp. Brain Res.* 86, 585~600.
 - 20) Girard, F., Venail, J., Schwaller, B. and Celio, M. R. (2015). The EF-hand Ca^{2+} -binding protein super-family: A genome-wide analysis of gene expression patterns in the adult mouse brain. *Neuroscience.* 294, 116~155.
 - 21) Glezer, I. I., Hof, P. R. and Morgane, P. J. (1992). Calretinin-immunoreactive neurons in the primary visual cortex of dolphin and human brains. *Brain Res.* 595,

181~188.

- 22) Gonchar, Y. and Burkhalter, A. (1997). Three distinct families of GABAergic neurons in rat visual cortex. *Cereb. Cortex.* 7, 347~358.
- 23) Gonchar, Y., Wang, Q. and Burkhalter, A. (2007). Multiple distinct subtypes of GABAergic neurons in mouse visual cortex identified by triple immunostaining. *Front. Neuroanat.* 1, 3.
- 24) Gonzalez-Burgos, G. and Lewis, D. A. (2008). GABA neurons and the mechanisms of network oscillations: implications for understanding cortical dysfunction in schizophrenia. *Schizophr. Bull.* 34, 944~61.
- 25) Haider, B. and McCormick, D. A. (2009). Rapid neocortical dynamics: cellular and network mechanisms. *Neuron.* 62, 171~189.
- 26) Higo, S., Udaka, N. and Tamamaki, N. (2007). Long-range GABAergic projection neurons in the cat neocortex. *J. Comp. Neurol.* 503, 421~431.
- 27) Hof, P. R., Bogaert, Y. E., Rosenthal, R. E. and Fiskum, G. (1996). Distribution of neuronal populations containing neurofilament protein and calcium-binding proteins in the canine neocortex: regional analysis and cell typology. *J. Chem. Neuroanat.* 11, 81~98.
- 28) Hof, P. R., Glezer, I. I., Condé, F., Flagg, R. A., Rubin, M. B., Nimchinsky, E. A. and Vogt Weisenhorn, D. M. (1999). Cellular distribution of the calcium-binding proteins parvalbumin, calbindin, and calretinin in the neocortex of mammals: phylogenetic and developmental patterns. *J. Chem. Neuroanat.* 16, 77~116.
- 29) Hof, P. R., Lüth, H. J., Rogers, J. H. and Celio, M. R. (1993). Calcium-binding proteins define subpopulations of interneurons in cingulate cortex.. *In*: Vogt, B.A, and Gabriel, M, [eds] *Neurobiology of Cingulate Cortex and Limbic Thalamus*, 1st ed., pp. 181~205. Birkhäuser, Boston.

- 30) Kawaguchi, Y. and Kondo, S. (2002). Parvalbumin, somatostatin and cholecystikinin as chemical markers for specific GABAergic interneuron types in the rat frontal cortex. *J. Neurocytol.* 31, 277~287.
- 31) Kirkcaldie, M. T. K. (2012). Neocortex. *In*: Watson, C. Paxinos, G. and Puelles, L. [eds] *The Mouse Nervous System*, 1st ed., pp. 52~92. Elsevier Academic Press, Amsterdam.
- 32) Kisler, L. B., Granovsky, Y., Sinai, A., Sprecher, E., Shamay-Tsoory, S. and Weissman-Fogel, I. (2016). Sex dimorphism in a mediatory role of the posterior midcingulate cortex in the association between anxiety and pain sensitivity. *Exp. Brain Res.* 234, 3119~3131.
- 33) Kubota, Y., Hattori, R. and Yui, Y. (1994). Three distinct subpopulations of GABAergic neurons in rat frontal agranular cortex. *Brain Res.* 649, 159~173.
- 34) Lee, J. E., Ahn, C. H., Lee, J. Y., Chung, E. S. and Jeon, C. J. (2004). Nitric oxide synthase and calcium-binding protein-containing neurons in the hamster visual cortex. *Mol. Cells.* 18, 30~39.
- 35) Levitt, P., Eagleson, K. L. and Powell, E. M. (2004). Regulation of neocortical interneuron development and the implications for neurodevelopmental disorders. *Trends Neurosci.* 27, 400~406.
- 36) Lewit-Bentley, A. and Réty, S. (2000). EF-hand calcium-binding proteins. *Curr. Opin. Struct. Biol.* 10, 637~643.
- 37) Markram, H., Toledo-Rodriguez, M., Wang, Y., Gupta, A., Silberberg, G. and Wu, C. (2004). Interneurons of the neocortical inhibitory system. *Nat. Rev. Neurosci.* 5, 793~807.
- 38) McBain, C. J. and Fisahn, A. (2001). Interneurons unbound. *Nat. Rev. Neurosci.* 2, 11~23.

- 39) Meskenaite, V. (1997). Calretinin-immunoreactive local circuit neurons in area 17 of the cynomolgus monkey, *Macaca fascicularis*. J. Comp. Neurol. 379, 113~132.
- 40) Miyoshi, G., Machold, R. P. and Fishell, G. (2013). Specification of GABAergic neocortical interneurons. In: Kageyama, R. Yamamori, T, [eds] Cortical Development: Neural Diversity and Neocortical Organization, 1st ed., pp. 89~126. Springer Japan, Tokyo.
- 41) Nakagawa, S., Takeuchi, H., Taki, Y., Nouchi, R., Sekiguchi, A., Kotozaki, Y., Miyauchi, C. M., Iizuka, K., Yokoyama, R., Shinada, T., Yamamoto, Y., Hanawa, S., Araki, T., Hashizume, H., Kunitoki, K., Sassa, Y. and Kawashima, R. (2017). The anterior midcingulate cortex as a neural node underlying hostility in young adults. Brain Struct. Funct. 222, 61~70.
- 42) Nieuwenhuys, R. (1994). The neocortex. An overview of its evolutionary development, structural organization and synaptology. Anat. Embryol. 190, 307~337.
- 43) Nimchinsky, E. A., Vogt, B. A., Morrison, J. H. and Hof, P. R. (1997). Neurofilament and calcium-binding proteins in the human cingulate cortex. J. Comp. Neurol. 384, 597~620.
- 44) Park, H. J., Kong, J. H., Kang, Y. S., Park, W. M., Jeong, S. A., Park, S. M., Lim, J. K. and Jeon, C. J. (2002). The distribution and morphology of calbindin D28K- and calretinin-immunoreactive neurons in the visual cortex of mouse. Mol. Cells. 14, 143~149.
- 45) Park, H. J., Lee, S. N., Lim, H. R., Kong, J. H. and Jeon, C. J. (2000). Calcium-binding proteins calbindin D28K, calretinin, and parvalbumin immunoreactivity in the rabbit visual cortex. Mol. Cells. 10, 206~212.
- 46) Paxinos, G., Watson, C., Carrive, P., Kirkcaldie, M. and Ashwell, K. W. S. (2009).

Chemoarchitectonic Atlas of the Rat Brain, 2nd ed., Elsevier Academic Press, Amsterdam.

- 47) Pereira, M. G., de Oliveira, L., Erthal, F. S., Joffily, M., Mocaiber, I. F., Volchan, E. and Pessoa, L. (2010). Emotion affects action: Midcingulate cortex as a pivotal node of interaction between negative emotion and motor signals. *Cogn. Affect. Behav. Neurosci.* 10, 94~106.
- 48) Pouille, F. and Scanziani, M. (2001). Enforcement of temporal fidelity in pyramidal cells by somatic feed-forward inhibition. *Science*. 293, 1159~1163.
- 49) Raghanti, M. A., Spocter, M. A., Butti, C., Hof, P. R. and Sherwood, C. C. (2010). A comparative perspective on minicolumns and inhibitory GABAergic interneurons in the neocortex. *Front. Neuroanat.* 4, 1~10.
- 50) Rogers, J. H. and Résibois, A. (1992). Calretinin and calbindin-D28k in rat brain: Patterns of partial co-localization. *Neuroscience*. 51, 843~865.
- 51) Rudy, B., Fishell, G., Lee, S. and Hjerling-Leffler, J. (2011). Three groups of interneurons account for nearly 100% of neocortical GABAergic neurons. *Dev. Neurobiol.* 71, 45~61.
- 52) Saxena, S., O'Neill, J. and Rauch, S. L. (2009). The role of cingulate cortex dysfunction in obsessive compulsive disorder. *In: Vogt, B. A., [ed.] Cingulate neurobiology and disease*, 1st ed., pp. 588~617. Oxford University Press, London.
- 53) Schwaller, B. 2014. Calretinin: from a “simple” Ca²⁺ buffer to a multifunctional protein implicated in many biological processes. *Front. Neuroanat.* 8, 1~7.
- 54) Shipp, S. (2007). Structure and function of the cerebral cortex. *Curr. Biol.* 17, R443-449.
- 55) Sikes, R. W., Vogt, L. J. and Vogt, B. A. (2008). Distribution and properties of visceral nociceptive neurons in rabbit cingulate cortex. *Pain*. 135, 160~174.

- 56) Tamamaki, N. and Tomioka, R. (2010). Long-range GABAergic connections distributed throughout the neocortex and their possible function. *Front. Neurosci.* 4, 202.
- 57) Tamamaki, N., Yanagawa, Y., Tomioka, R., Miyazaki, J. I., Obata, K. and Kaneko, T. (2003). Green fluorescent protein expression and colocalization with calretinin, parvalbumin, and somatostatin in the GAD67-GFP knock-in mouse. *J. Comp. Neurol.* 467, 60~79.
- 58) Tomioka, R., Okamoto, K., Furuta, T., Fujiyama, F., Iwasato, T., Yanagawa, Y., Obata, K., Kaneko, T. and Tamamaki, N. (2005). Demonstration of long-range GABAergic connections distributed throughout the mouse neocortex. *Eur. J. Neurosci.* 21, 1587~1600.
- 59) Vertes, R. P., Hoover, W. B., Do Valle, A. C., Sherman, A. and Rodriguez, J. J. (2006). Efferent projections of reuniens and rhomboid nuclei of the thalamus in the rat. *J. Comp. Neurol.* 499, 768~796.
- 60) Vogt, B. A., Berger, G. R. and Derbyshire, S. W. G. (2003). Structural and functional dichotomy of human midcingulate cortex. *Eur. J. Neurosci.* 18, 3134~3144.
- 61) Vogt, B. A., Sikes, R. W., Swadlow, H. A. and Weyand, T. G. (1986). Rabbit cingulate cortex: Cytoarchitecture, physiological border with visual cortex, and afferent cortical connections of visual, motor, postsubicular, and intracingulate origin. *J. Comp. Neurol.* 248, 74~94.
- 62) Vogt, B. A. (1993). Structural organization of cingulate cortex: areas, neurons, and somatodendritic transmitter receptors.. *In: Vogt, B.A, and Gabriel, M, [eds] Neurobiology of Cingulate Cortex and Limbic Thalamus, 1st ed., pp. 19~70. Birkhäuser, Boston.*

- 63) Vogt, B. A. (2016). Cytoarchitecture and neurocytology of rabbit cingulate cortex. *Brain Struct. Funct.* 221, 3571~3589.
- 64) Vogt, B. A. (2016). Midcingulate cortex: Structure, connections, homologies, functions and diseases. *J. Chem. Neuroanat.* 74, 28~46.
- 65) Vogt, B. A. (2009). Architecture, neurocytology and comparative organization of monkey and human cingulate cortices. *In: Vogt, B. A., [ed] Cingulate neurobiology and disease*, 1st ed., pp. 65~91. Oxford University Press, New York.
- 66) Vogt, B. A. and Paxinos, G. (2014). Cytoarchitecture of mouse and rat cingulate cortex with human homologies. *Brain Struct. Funct.* 219, 185~192.
- 67) Vogt, B. A. and Sikes, R. W. 2009. Cingulate nociceptive circuitry and roles in pain processing: The cingulate premotor pain model. *In: Vogt, B. A., [ed] Cingulate neurobiology and disease*, 1st ed., pp. 331~333. Oxford University Press, New York.
- 68) Vogt, B. A., Vogt, L., Farber, N. B. and Bush, G. (2005). Architecture and neurocytology of monkey cingulate gyrus. *J. Comp. Neurol.* 485, 218~239.
- 69) Watson, C. and Paxinos, G. (2010). Chemoarchitectonic atlas of the mouse brain, 1st ed., Elsevier Academic Press, Amsterdam.
- 70) Wehr, M. and Zador, A. M. (2003). Balanced inhibition underlies tuning and sharpens spike timing in auditory cortex. *Nature.* 426, 442~446.
- 71) Winsky, L., Montpied, P., Arai, R., Martin, B. M. and Jacobowitz, D. M. (1992). Calretinin distribution in the thalamus of the rat: Immunohistochemical and in situ hybridization histochemical analyses. *Neuroscience.* 50, 181~196.
- 72) Xu, X., Roby, K. D. and Callaway, E. M. (2010). Immunochemical characterization of inhibitory mouse cortical neurons: three chemically distinct classes of inhibitory cells. *J. Comp. Neurol.* 518, 389~404.
- 73) Yu, C., Zhou, Y., Liu, Y., Jiang, T., Dong, H., Zhang, Y. and Walter, M. (2011).

Functional segregation of the human cingulate cortex is confirmed by functional connectivity based neuroanatomical parcellation. *Neuroimage*. 54, 2571~2581.

Fig. 1. The distribution of CR⁺ structures (a, b) and the corresponding areal and laminar patterns demonstrated with NeuN immunostaining (a', b') in the anterior (a, a') and the posterior MCC (b, b'). (c) shows the location of the MCC (= area 24') and the anteroposterior levels of the cutting planes of a/a' and b/b' (blue lines) in the medial view of the hemisphere. The dotted line shows the border between area a24' and area p24'. Arrowheads in a, a', b and b' denote areal boundaries. Bar represents 500 μ m, which is applicable to a, a', b and b'.

Fig. 1

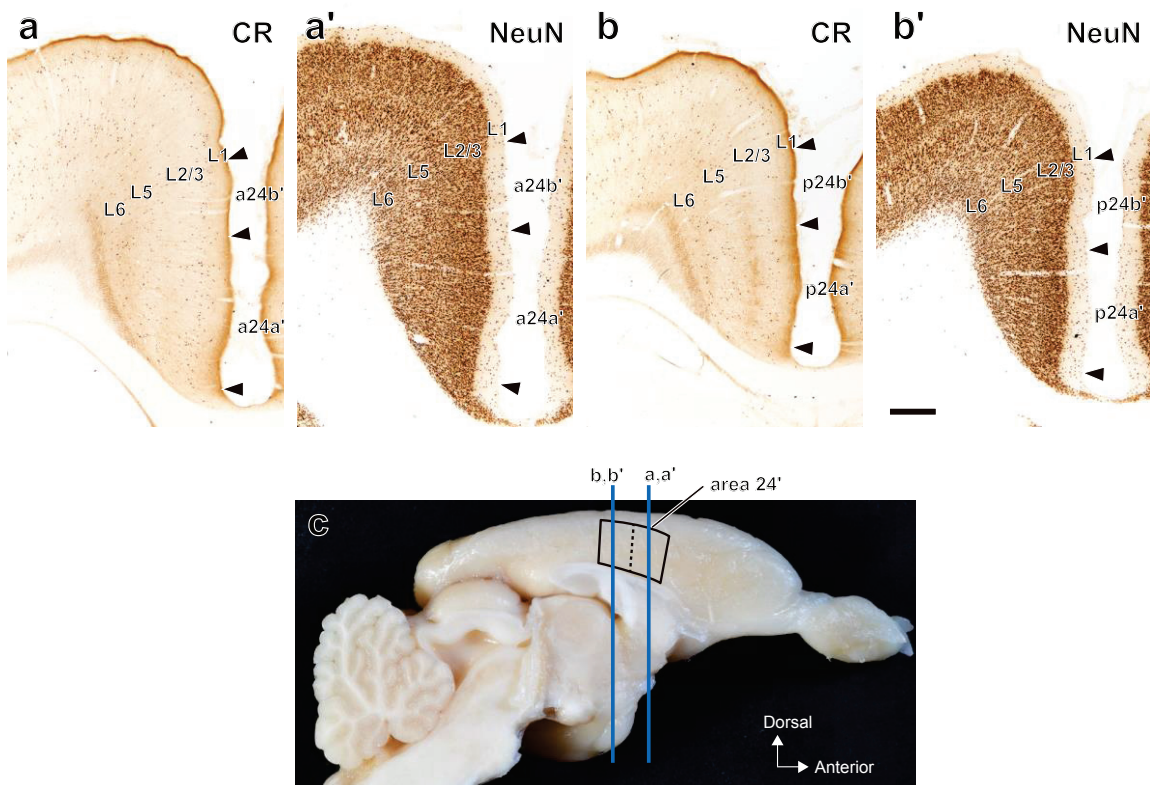


Fig. 2 CR+ structures in the areas of the MCC. (a) area a24a', (b) area p24a', (c) area a24b' and (d) area p24b'. CR+ somata are more numerous in L2/3 and L6 than in L1 and L5. Most of CR+ somata are of the multipolar and some are of the bipolar type. Arrowheads denote examples of the bipolar somata. CR+ fibers are densely distributed in superficial L1. Furthermore, in areas p24a' and p24b', CR+ fibers are present in patches in deep L2/3 (arrows), whereas they are not present in areas a24a' and a24b'. Thin bars denote laminar borders and the thick bar in (d) represents 200 μm , which is applicable to (a)-(c).

Fig. 2

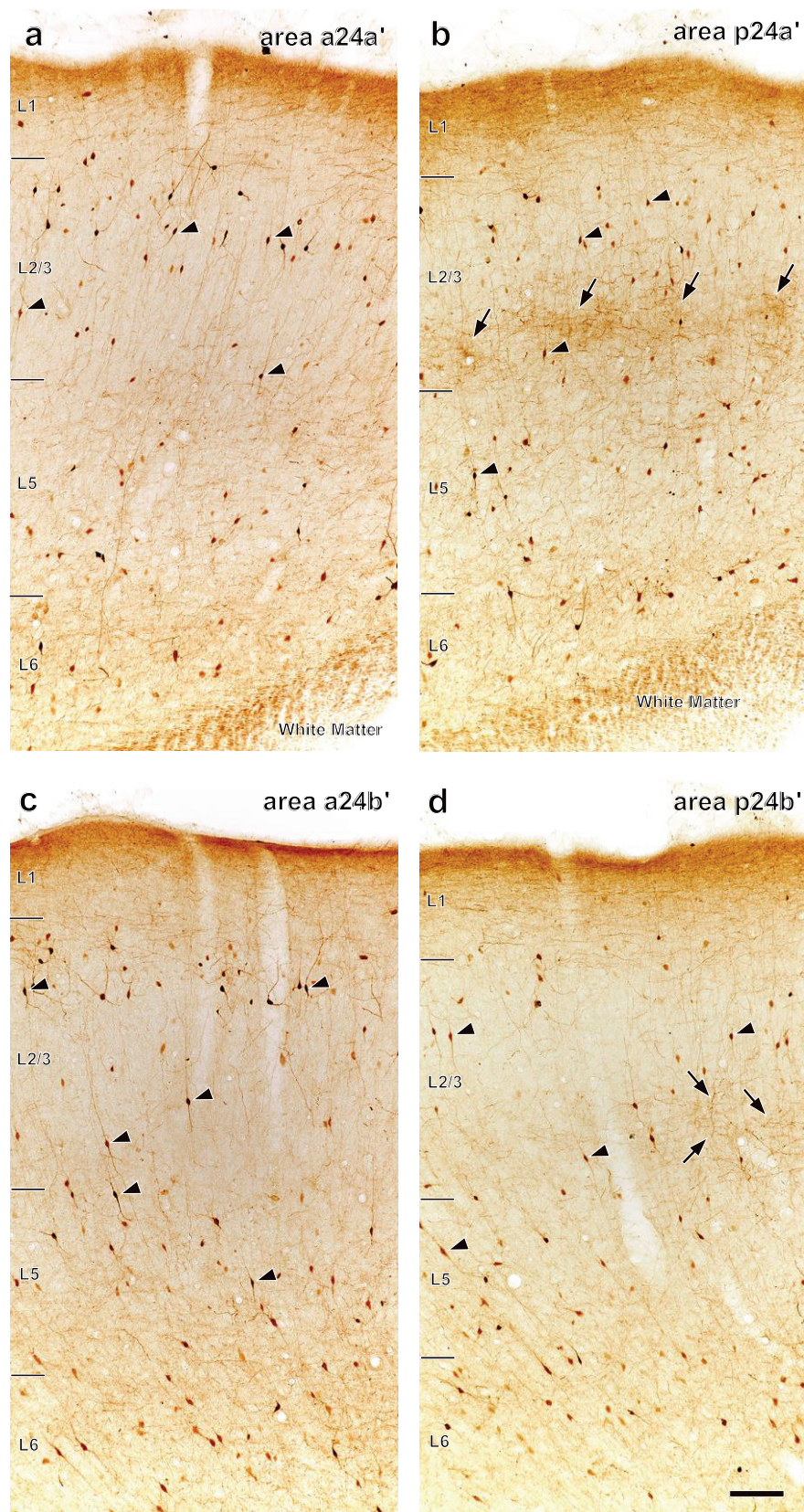


Fig. 3 Columnar graphs showing the statistical difference in number of CR+ somata in each MCC area. *, $P < 0.05$; **, $P < 0.01$; and ***, $P < 0.005$. BP = bipolar somata and MP = multipolar somata.

Fig. 3

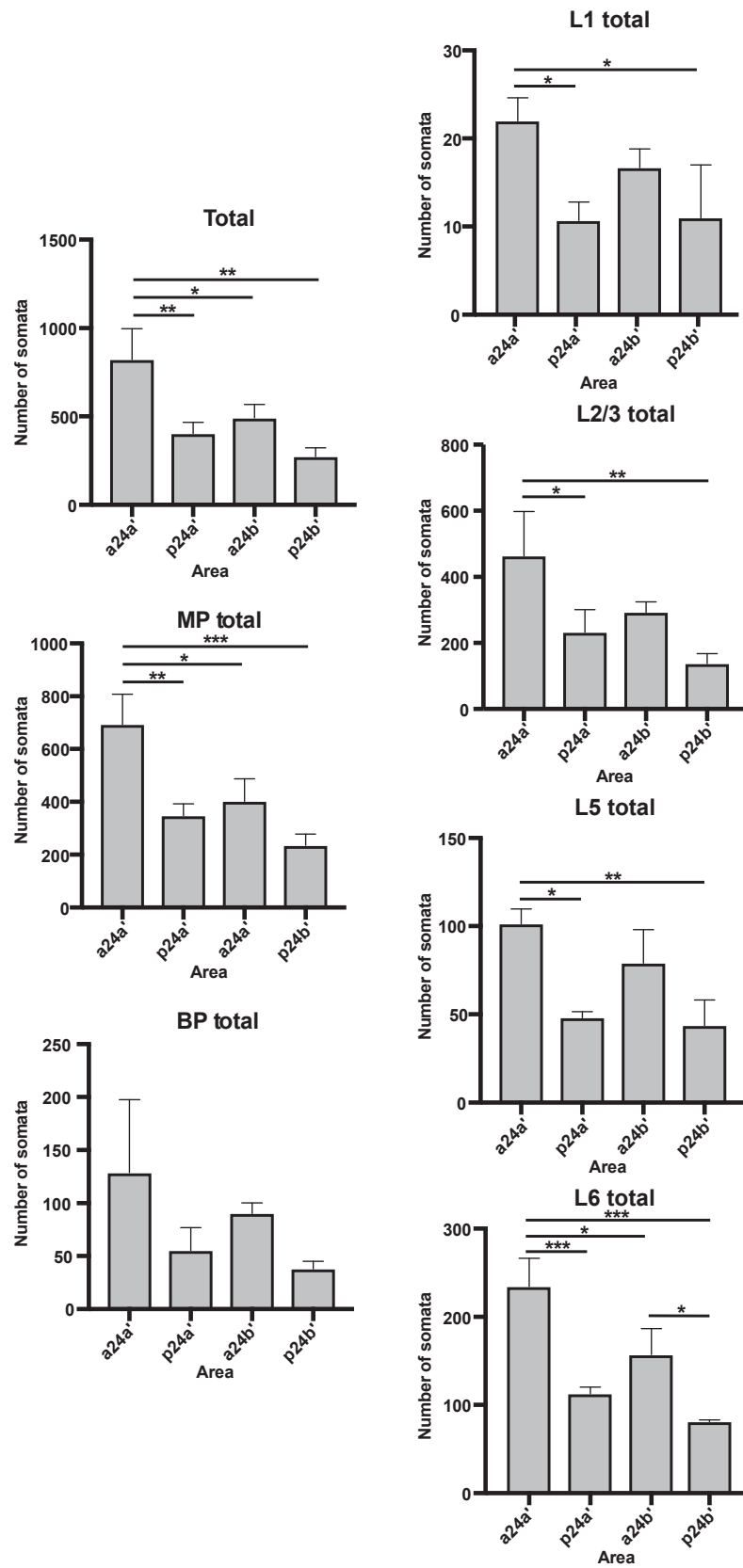


Fig. 4 Columnar graphs showing the statistical difference in density of CR+ somata in each MCC area. *, $P < 0.05$; **, $P < 0.01$; ***, $P < 0.005$; and ****, $P < 0.001$. BP = bipolar somata and MP = multipolar somata.

Fig.

4

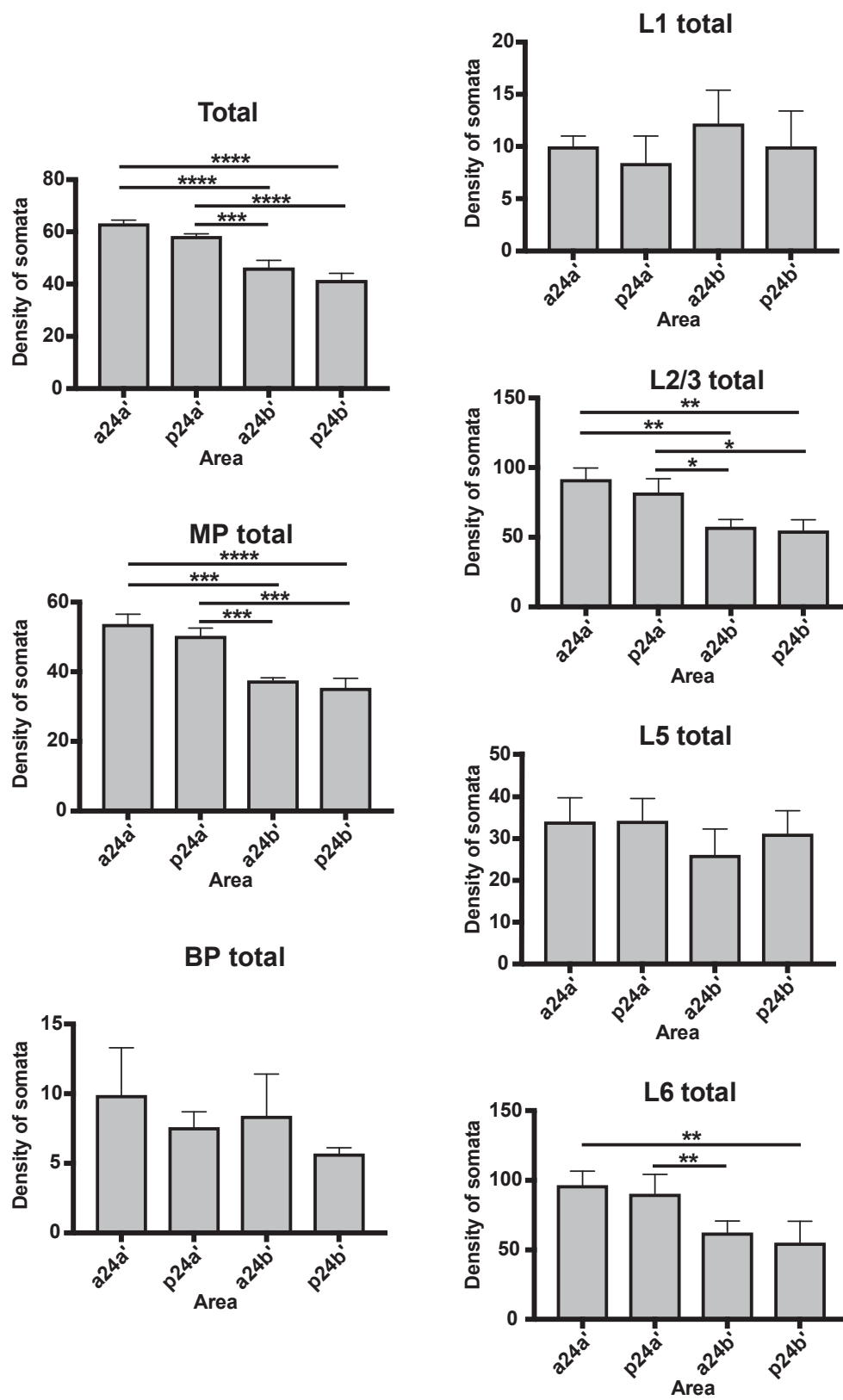


Fig. 5 Characteristics of CR+ somata and fibers. (a) CR+ multipolar (black arrowheads) and bipolar somata (white arrowheads) in superficial L2/3 of area a24a'. (b) Beaded dendritic processes (arrowheads) arising from a multipolar soma located in superficial L2/3 of area a24a'. (c) CR+ fibers in superficial L1 of area a24a'. A CR+ soma is also present in the deep part. (d) CR+ fibers in superficial L1 of area p24a'. These fibers are more abundant than those of area a24a'. (e) A patch of CR+ fibers and terminals (arrows) in deep L2/3 of area p24a'. (f) A higher view of part of the patch in (e), showing terminals (arrowheads). Bars represent 50 μ m.

Fig. 5

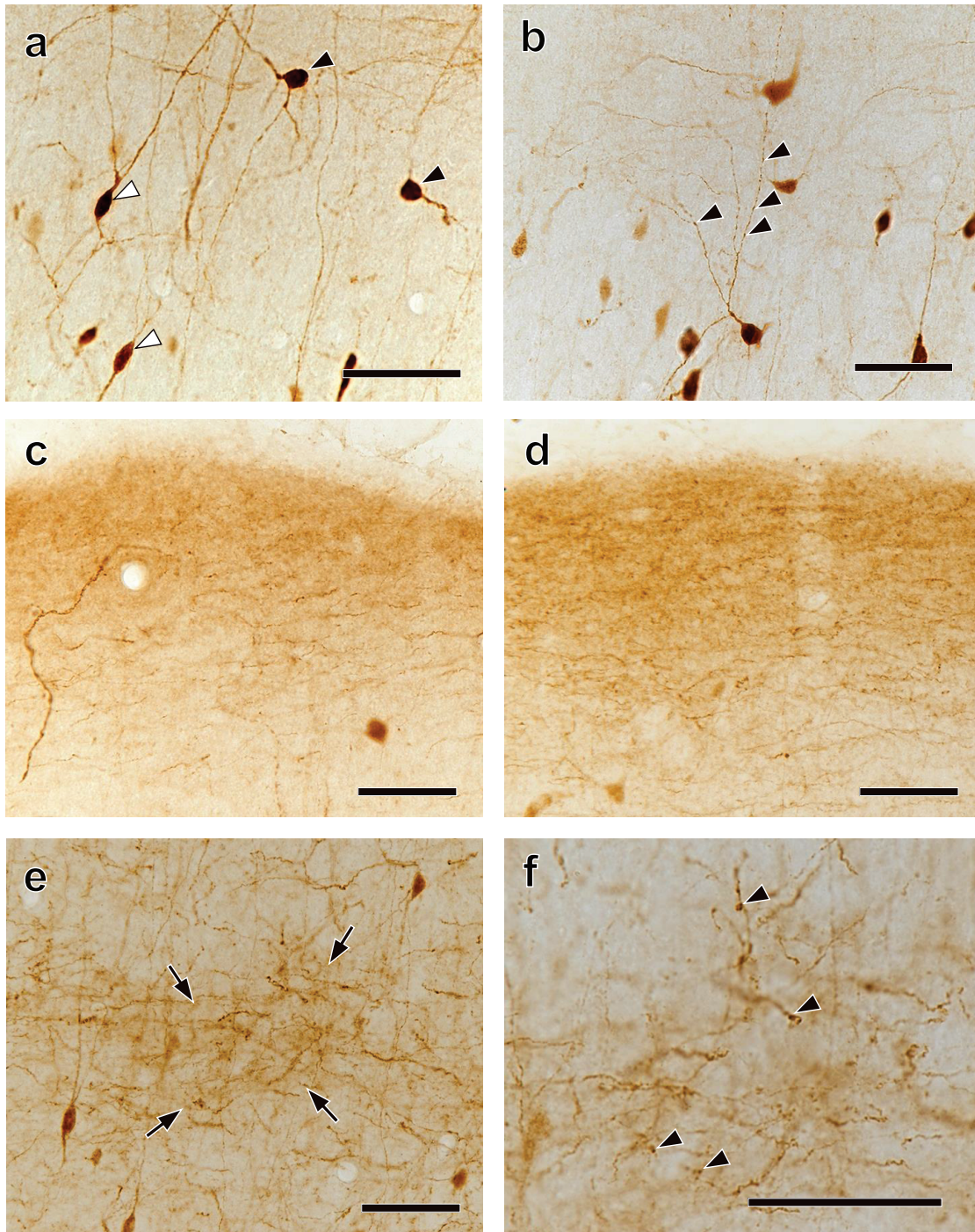


Table. 1 Number (mean \pm SD) of CR+ somata in each area/layer of the MCC

Layers	area a24a'			area p24a'			area a24b'			area p24b'		
	MP	BP	All somata	MP	BP	All somata	MP	BP	All somata	MP	BP	All somata
L1	22.0 \pm 2.6	0.0 \pm 0.0	22.0 \pm 2.6	10.7 \pm 2.1	0.0 \pm 0.0	10.7 \pm 2.1	16.7 \pm 2.1	0.0 \pm 0.0	16.7 \pm 2.1	11.0 \pm 6.0	0.0 \pm 0.0	11.0 \pm 6.0
L2/3	360.7 \pm 85.3	103.0 \pm 56.8	463.7 \pm 134.5	184.3 \pm 53.0	48.0 \pm 16.6	232.3 \pm 68.7	177.3 \pm 26.3	62.0 \pm 9.6	239.3 \pm 30.7	108.3 \pm 23.2	29.3 \pm 8.5	137.7 \pm 30.0
L5	86.7 \pm 6.8	13.0 \pm 6.9	99.7 \pm 11.1	42.7 \pm 3.2	5.3 \pm 3.1	48.0 \pm 3.6	61.0 \pm 23.1	18.0 \pm 5.2	79.0 \pm 19.0	36.7 \pm 14.6	7.0 \pm 6.6	43.7 \pm 14.5
L6	223.3 \pm 23.6	11.0 \pm 8.9	234.3 \pm 32.0	110.7 \pm 10.2	2.0 \pm 2.6	112.7 \pm 7.6	146.7 \pm 40.3	10.3 \pm 10.7	157.0 \pm 29.7	79.3 \pm 1.5	1.7 \pm 1.5	81.0 \pm 2.0
All layers	692.7 \pm 114.7	128.7 \pm 68.8	821.3 \pm 175.6	348.3 \pm 44.4	55.3 \pm 21.4	403.7 \pm 63.1	401.7 \pm 85.1	90.3 \pm 10.1	492.0 \pm 76.5	235.3 \pm 43.0	38.0 \pm 7.0	273.4 \pm 49.8

BP, bipolar, and MP, multipolar somata.

Table. 2 Density (n/mm^2 ; mean \pm SD) of CR+ multipolar and bipolar somata in each area/layer of the MCC

Layers	Area a24a'			Area p24a'			Area a24b'			Area p24b'		
	MP	BP	All somata	MP	BP	All somata	MP	BP	All somata	MP	BP	All somata
L1	10.0 \pm 1.0	0	10.0 \pm 1.0	8.4 \pm 3.2	0	8.4 \pm 2.6	12.2 \pm 3.1	0	12.2 \pm 3.2	10.0 \pm 3.0	0	10.0 \pm 3.4
L2/3	72.4 \pm 12.0	19.3 \pm 4.2	91.7 \pm 8.0	66.0 \pm 9.1	16.0 \pm 1.3	82.0 \pm 10.0	42.8 \pm 4.1	14.7 \pm 2.2	57.5 \pm 5.2	42.6 \pm 6.1	12.2 \pm 3.0	54.8 \pm 7.8
L5	29.1 \pm 1.2	5.0 \pm 2.2	34.1 \pm 5.7	30.0 \pm 3.2	4.3 \pm 2.0	34.3 \pm 5.3	23.9 \pm 2.2	8.1 \pm 2.0	26.1 \pm 6.2	24.8 \pm 2.4	6.4 \pm 2.1	31.2 \pm 5.5
L6	92.1 \pm 13.0	4.3 \pm 3.1	96.4 \pm 10.1	88.1 \pm 16.0	2.2 \pm 1.0	90.3 \pm 14.0	57.0 \pm 2.4	5.3 \pm 2.0	62.3 \pm 8.4	53.0 \pm 13.7	2.1 \pm 1.2	55.1 \pm 15.4
All layers	53.7 \pm 2.8	9.9 \pm 3.4	63.6 \pm 1.2	50.3 \pm 2.2	7.6 \pm 1.1	58.4 \pm 0.9	37.5 \pm 0.8	8.4 \pm 3.0	46.3 \pm 2.7	35.4 \pm 2.7	5.7 \pm 0.4	41.5 \pm 2.6

BP, bipolar, and MP, multipolar somata.

